The regulation of polar flagella assembly in *Pseudomonas putida*

Marta Pulido-Sánchez[1], Antonio Leal-Morales[1], Aroa López-Sánchez[1], Felipe Cava[2] and Fernando Govantes[1]*

Running title: Regulation of flagellar assembly

[1]Centro Andaluz de Biología del Desarrollo, Universidad Pablo de Olavide/Consejo Superior de Investigaciones Científicas/Junta de Andalucía and Departamento de Biología Molecular e Ingeniería Bioquímica, Universidad Pablo de Olavide, Sevilla, Spain.

[2]The Laboratory for Molecular Infection Medicine Sweden (MIMS), Umeå Center for Microbial Research (UCMR), Science for Life Laboratory (SciLifeLab), Department of Molecular Biology, Umeå University, Umeå, Sweden.

*Corresponding author. Address: Centro Andaluz de Biología del Desarrollo, Universidad Pablo de Olavide, Carretera de Utrera, Km. 1, 41013, Sevilla, Spain. Phone: +34 954349386. Fax: +34 954349376. E-mail: fgovrom@upo.es

ABSTRACT

The Gram-negative bacterium *Pseudomonas putida* bears a tuft of flagella at a single cell pole. New flagella must be assembled *de novo* every cell cycle to secure motility of both daughter cells. Here we show that the coordinated action of FimV, FlhF and FleN sets the location, timing and number of flagella assembled. The polar landmark protein FimV recruits FleN and enables stable association of FlhF to the cell poles. FlhF determines flagellar position by recruiting FliF to the cell pole and preventing its nucleation at non-polar sites. FlhF is also required for assembly of the flagellar type III secretion system, enabling Class III flagellar promoter activation and export of the external flagellar components. FleN regulates flagellar number by repressing *flhF* expression and a second, posttranscriptional mechanism. Flagellar assembly starts with FlhF recruitment to the new pole shortly after cell division and finishes with the emergence of FliC filaments during the following cell division. FimV and FleN regulate the onset of flagellar assembly by preventing premature polar targeting of FlhF. Our results shed new light on the mechanisms that ensure the timely assembly of the appropriate number of flagella at the correct polar location in polarly flagellated bacteria.

INTRODUCTION

For many bacteria, the planktonic stage is hallmarked by the synthesis of one or more flagella, intricate molecular engines that enable motility in a liquid or semi-solid medium by engaging in propeller-like rotation (Altegoer *et al.,* 2014). Flagella are made of three functional units: the basal body, a rotary machine embedded in the cell envelope; the filament, a long and thin helical structure that protrudes from the cells and acts as a propeller; and the hook, a rigid, curved element that connects basal body and filament. The basal body is in turn made out of five structural elements: the membrane-bound MS-ring lends support to the rest of components; the cytoplasmic C-ring modulates the direction of flagellar rotation; the flagellar type III secretion system (fT3SS) exports the extracellular flagellar

components; the rod is a hollow cylinder that acts as a drive shaft for rotation and connects the MS-ring and the hook; and the cell wall-bound LP-ring surrounds the rod and plays the role of bushing. The flagellar stator, a membrane-bound complex that couples proton transport to the generation of torque is associated to the periphery of the basal body (Chevance & Hughes, 2008; Terashima *et al.*, 2008). Flagellar function is modulated by the chemotaxis complexes, containing specific chemoreceptors and signal transduction proteins that interact with the C-ring to promote directional motion in response to concentration gradients (Matilla & Krell, 2017). The flagellar apparatus is sequentially assembled from the inside out (Chevance & Hughes, 2008), and flagellar genes are regulated by transcriptional cascades whose logic mirrors this assembly hierarchy (Smith & Hoover, 2009). Exquisite regulation of this process is paramount, as the synthesis and operation cost of the flagellar/chemotaxis system represents a substantial fraction of the energy resources of the cell (Macnab, 1996; Martínez-García *et al.*, 2014).

Bacterial flagellation patterns are diverse and genetically determined in a species-specific fashion. Peritrichous flagella are located along the bacterial cell. Polar flagella may occur as single units in one (monotrichous) or both poles (amphitrichous), or as tufts containing a variable number of flagella (lophotrichous) in one or both poles. Less commonly, bacterial species naturally bearing their flagella in lateral or subpolar positions have also been described (Leifson, 1951; Schuhmacher *et al.*, 2015). In peritrichously flagellated bacteria, such as *Escherichia coli*, flagella are assembled around the cell body and cell division results in a more or less even distribution of the existing flagella between both daughter cells to allow effective motility (Schuhmacher *et al.*, 2015). In contrast, in bacteria displaying an unipolar flagellation pattern only one of the daughter cells inherits the preexisting flagellar machinery after cell division, and a new set of flagella must be assembled at the opposite pole to support motility of the other daughter cell (Amako & Umeda, 1982). To this end, cells must deploy specific regulatory mechanisms to ensure the

correct location and number of flagella and precise timing to match the emergence of the new functional flagella with the completion of cell division. Much like chromosome replication and segregation, the synthesis and assembly of unipolar flagella can be envisioned as a discontinuous process that must be initiated in each cell cycle and terminated concomitantly to cell division.

Pseudomonas putida is a well-characterized Gram-negative soil bacterium endowed with great metabolic versatility and a model organism for biodegradation of organic toxicants and bioremediation (Martins dos Santos *et al.*, 2004). During planktonic growth, *P. putida* displays unipolar lophotrichous flagellation. Most flagellar and core chemotaxis genes are located in a single chromosomal region, known as the flagellar cluster. Our recent work has unveiled the transcriptional organization of the flagellar cluster and the regulation of the flagellar gene set by a three-tiered regulatory cascade (Leal-Morales *et al.*, 2021). FleQ is the master regulator of the flagellar/chemotaxis system in *P. putida*. FleQ activates σ^{54}-dependent Class II flagellar promoters to drive the synthesis of all the structural components of the basal body and hook, and part of the core chemotaxis apparatus. FleQ also activates the synthesis of the alternative σ factor FliA. FliA is directly accountable for the activation of all the remaining (Class III) flagellar promoters (Leal-Morales *et al*., 2021), and multiple chemoreceptor-encoding genes (Rodríguez-Herva *et al.*, 2010; Marta Pulido-Sánchez, unpublished results).

The *P. putida* flagellar cluster encodes at least two proteins potentially involved in the spatial, temporal and numerical regulation of flagellar synthesis. The MinD-like ATPase FleN (also known as FlhG or YlxH), and the SRP family GTPase FlhF are major players in determining the location and number of flagella in numerous bacterial species. FlhF is generally considered as a landmark protein that determines polar location of the flagella, while FleN is a negative regulator that limits the number of flagella (reviewed by Kazmierczak & Hendrixson, 2013; Altegoer *et al.*, 2014; Schuhmacher *et al.*, 2015). Our

recent work has shown that deletion of *flhF* in *P. putida* results in the assembly of a single flagellum at a random position, while deletion of *fleN* leads to hyperflagellated cells with a unipolar lophotrichous pattern (Navarrete *et al*., 2019). FleN is also an antagonist of FleQ activation of the Class II flagellar promoters and *fleN* deletion provokes the overexpression of multiple flagellar genes (Navarrete *et al*., 2019; Leal-Morales *et al*., 2022).

P. putida genomes also encode orthologs of FimV, a *Pseudomonas aeruginosa* polar landmark protein. *P. aeruginosa* FimV promotes polar assembly of type IV pili (Carter *et al*., 2017), contributes to the activation of virulence genes *via* cAMP-mediated signaling (Inclan *et al*., 2016) and regulates the planktonic to biofilm transition (Bense *et al*., 2019; Schniederberend *et al*., 2019; Nicastro *et al*., 2020). FimV-related proteins, designated FimV, HubP or TspA, are present in multiple species of β- and γ-proteobacteria (Buensuceso *et al*., 2016). Members of the FimV/HubP/TspA family share a conserved architecture consisting of a N-terminal periplasmic domain, a single transmembrane region and a C-terminal cytoplasmic domain, but sequence conservation is limited to a periplasmic peptidoglycan-binding LysM motif (**IPR018392**) and a ~50 residue distal C-terminal motif (**IPR020011**) (Wehbi *et al*., 2011; Buensuceso *et al*., 2017). HubP proteins from *Vibrio and Shewanella* spp. are polar landmarks involved in flagellar and chemotaxis complex biogenesis and replication origin segregation among others (Yamaichi *et al*., 2012; Rossmann *et al*., 2015 Takekawa *et al*., 2016; Arroyo-Pérez & Ringgaard, 2021; Altinoglu *et al*., 2022; Rick *et al*., 2022).

Here we demonstrate the involvement of FlhF, FleN and FimV in the temporal, spatial and numerical regulation of flagellar biogenesis in *P. putida*. Our results suggest that the recruitment of FimV, FlhF and FleN to the new pole shortly after cell division is required for the timely assembly of the correct number of flagella at the appropriate polar location. These findings shed light on the complex regulatory mechanisms required to ensure the faithful inheritance of the motile phenotype by both daughter cells in unipolarly flagellated bacteria.

MATERIALS AND METHODS

Bacterial strains and growth conditions

Bacterial strains used in this work are listed in **Supplemental Table S1**. Liquid cultures of *E. coli* and *P. putida* were routinely grown in Luria-Bertani (LB) medium (Sambrook & Russell, 2000) at 37 ºC and 30 ºC, respectively, with 180 rpm shaking. For solid media, American Bacteriological Agar (Condalab) was added to a final concentration of 15 g l^{-1}. When needed, antibiotics and other compounds were added at the following concentrations: ampicillin (100 mg l^{-1}), carbenicillin (500 mg l^{-1}), chloramphenicol (15 mg l^{-1}), rifampicin (20 mg l^{-1}), gentamycin (10 mg l^{-1}), kanamycin (25 mg l^{-1}), 3-methylbenzoate (3MB) (3 mM) and sodium salicylate (2 mM). All reagents were purchased from Sigma-Aldrich.

Plasmid and strain construction

Plasmids and oligonucleotides used in this work are summarized in **Supplemental Table S1.** All DNA manipulations were performed following standard protocols (Sambrook & Russell, 2000). Restriction and modification enzymes were used following to the manufacturer's instructions (New England Biolabs). PCR amplifications were carried out using Q5® High-Fidelity DNA Polymerase (New England Biolabs) for cloning and DreamTaq™ DNA Polymerase (Thermo Fisher) to verify plasmid constructions and chromosomal manipulations. One-step isothermal dsDNA Gibson assembly was performed as described (Gibson, 2011). *E. coli* DH5α was used as host strain for cloning procedures. Cloning steps involving PCR were verified by commercial Sanger sequencing (Stab Vida). Plasmid DNA was transferred to *E. coli* strains by transformation (Inoue *et al*., 1990), and to *P. putida* by triparental mating (Espinosa-Urgel *et al*., 2000) or electroporation (Choi *et al*., 2006). Site-specific integration of miniTn7-derivatives in *P. putida* strains was performed as previously described (Choi *et al*., 2005), and PCR-verified. Specific details of plasmid and strain construction are provided as **Supplementary Materials and Methods**.

Swimming and swarming motility assays

Swimming assays were adapted from Parkinson (1976). Fresh colonies were toothpick-inoculated in Tryptone-agar plates (1 % Bacto™ Tryptone [Difco], 0.5 % NaCl, 0.3 % Bacto™ Agar), and incubated at 30 ºC for 12 h. Digital images were taken and swimming halos diameter were measured using GIMP v2.10.12 (https://www.gimp.org) and normalized to the wild-type. At least, three biological replicates were assayed for each strain.

***In vivo* gene expression assays**

End-point fluorescence measurements were taken to quantify gene expression in strains harboring *gfp-lacZ* transcriptional fusions to different promoters. Overnight LB cultures supplemented with the corresponding antibiotics were diluted in 3 mL of the same medium to an A_{600} of 0.01 and incubated at 30 ºC with 180 rpm shaking until reaching A_{600} of 0.4-0.6 (exponential phase). Samples of 1 mL were withdrawn and cells were washed three times in phosphate-buffered saline (PBS). Cells were resuspended in 500 µL of PBS and 150 µL were dispensed by triplicate into the wells of Costar® 96-well polystyrene plates (Corning). A_{600} and GFP fluorescence (485 nm excitation, 535 nm emission, gain value set to 55) were measured in a Tecan Spark 10M microplate reader. Three biological replicates were assayed for each strain.

Protein secretion assay

Overnight cultures of strains expressing FlgM-FLAG were 100-fold diluted in 50 mL of LB medium supplemented with 2 mM salicylate and grown to A_{600} of 4. Cells were harvested by centrifugation (5000 *g*, 4 ºC, 15 min) and culture supernatants were collected for further precipitation. To increase the detection threshold in the intracellular fraction, pelleted cells were resuspended in 5 mL of cold buffer B (20 mM Tris-HCl pH 8.0, 150 mM NaCl, 0.5 % Nonidet P-40) and disrupted by sonication. Soluble fractions were rotating-incubated overnight at 4 ºC with 20 µL of buffer-equilibrated Anti-FLAG® M2 magnetic beads (Sigma-Aldrich), followed by 10 washes with 1 mL of the same buffer. Culture supernatants

were filtered through Millipore membranes with 0.45 μM pore-size (Merck) and TCA was added to a final concentration of 10 % (v/v). After overnight incubation at 4 ºC, precipitates were collected by centrifugation (8000 *g*, 4 ºC, 30 min) and washed 3 times with 1 mL cold acetone. Protein pellets were dried for 10 min at 100 ºC. Precipitated supernatants and immunoprecipitated soluble cell fractions were further analyzed by Western-Blot.

SDS-PAGE and Western-Blot analysis

Protein samples were mixed with 2x loading buffer (150 mM Tris-HCl pH 6.8, 20 % glycerol, 4% SDS, 0.1 % bromophenol blue, 10 % β-mercaptoetanol) and boiled at 100 ºC for 10 min. Samples were centrifuged at 18000 *g* for 1 min and supernatants were separated on 12.5 % SDS-PAGE gels. Proteins were transferred to nitrocellulose membranes using a Trans-Blot Turbo Transfer System (Bio Rad). Membrane was blocked for 2 h at room temperature in blocking solution (3 % fat-free milk in TBS buffer with 1 % Tween 20). Blocked membrane was incubated overnight at 4 ºC with primary antibody anti-FLAG (F3165, Sigma-Aldrich, 1:2000 dilution), washed 3 times in TBS with 1% Tween 20 (TBS-T), probed for 2 h at 4 ºC with secondary antibody anti-mouse HRP-conjugated (31430, Thermo Fischer, 1:10000 dilution), and washed with TBS-T as before. Membranes were added Pierce™ ECL Western Blotting Substrate (Thermo Fischer) and chemiluminescent signal was revealed using a ChemiDoc MP instrument (Bio-Rad) with a exposure time of 800 s. Image Lab software (Bio-Rad) was employed for image analysis.

Time-lapse fluorescence microscopy

Overnight cultures were 100-fold diluted in LB medium and grown to early-exponential phase (A_{600} of 0.2-0.3). Culture drops (2 μL) were placed on LB-agarose pads (1 % [w/v] agarose in 10 % [v/v] LB, to minimize background fluorescence) in glass slides and cells were imaged every 5 min using an Axio Imager.Z2 (Zeiss) microscope equipped with a Plan-Apochromat 63x/1.40 Oil Ph 3 M27 contrast objective lens and an ORCA-Flash 4.0 LT digital CMOS camera (Hamamatsu, pixel size: 0.1031 μm), controlled by the Zeiss

ZEN 2 (Blue edition) software enabling software autofocus for focus maintenance over time. Phase contrast and GFPmut3 fluorescence images were respectively acquired using a TL Vis-LED Lamp (4.91 Volt, exposure time of 50 ms) and the LED module 470 nm from a Colibri.2 LED light source using a Zeiss 38 HE Green Fluorescent Prot. filter (excitation filter BP: 450/490 nm, emission filter BP: 500/550 nm, exposure time of 500 ms).

Confocal microscopy

Overnight cultures were 100-fold diluted in LB medium supplemented with 2 mM salicylate when necessary and grown to exponential phase (A_{600} of 0.4-0.6). Cells from 1 mL samples were harvested by centrifugation at 5000 *g* for 5 min and washed three times in PBS to remove LB. Flagellar filaments of strains expressing $FliC^{S267C}$ were stained by gently resuspending cells in 50 µL of PBS containing 5 µg/mL Alexa Fluor™ 488 C_5 maleimide (Molecular Probes), followed by incubation for 5 min at room temperature in the dark (Hintsche *et al*., 2017). Cells were washed three times for excess dye removal. For membrane staining, cells were resuspended in 100 µL of PBS containing 5 µg/mL FM™ 4-64 (Molecular Probes). After incubation for 5 min at room temperature in the dark, 2 µL drops were immediately placed on 1 % agarose pads made with deionized water to be imaged using an Axio Observer7 confocal microscope (Zeiss) equipped with a CSU-W1 spinning disk module (Yokogawa). Images were taken using a Zeiss α Plan-Apochromat 100x/1.46 Oil DIC M27 objective lens and a Prime 95B CMOS camera (Teledyne Photometrics, pixel size: 0.1099 µm), controlled by the SlideBook 6 software. GFPmut3 and Alexa Fluor™ 488-labeled $FliC^{S267C}$ fluorescence was excited with the 488 nm laser line and collected with emission filter 525/50 nm, while FM™ 4-64 was excited at 561 nm and collected with a 617/73 filter (exposure time of 1000 ms). Exposure times for GFPmut3-tagged FimV, FlhF, FliF and FliM were 300 ms, 1000 ms for FleN and 100 ms for Alexa Fluor™ 488-labeled $FliC^{S267C}$. For each image, 7 Z-sections were collected with a step size of 0.33 µm.

Microscopy image analysis

Microscopy images processing and analysis were performed using Fiji software v1.53t (Schneider *et al*., 2015). Background subtraction of the fluorescence signal from GFPmut3, Alexa Fluor™ 488 C_5 maleimide and FM™ 4-64 was set to a rolling ball radius of 20 pixels. Confocal images are shown as maxima projections of 7 Z- sections of the 525/50 channel, merged with the 617/73 channel showing the focal plane with the cell contour. Cell segmentation, maxima and foci detection, and cell measurements from confocal images were performed using MicrobeJ v5.13I plugin (Ducret *et al*., 2016). Unless otherwise stated, default parameters were applied. Cell perimeter detection was performed on the lowest Z-plane of the brightfield channel using the rod-shaped descriptor (area: 1-9 μm^2, length: 2-5.5 µm, width: 0.5-3 µm). The old cell pole was defined as the one showing the highest maxima intensity from the 525/50 channel. Images showing the same fluorescence-labeled protein were batched-processed using the same maxima/foci tolerance and Z-score parameters, with a minimal intensity cutoff value of 200 and foci area of 0.02-max μm^2. A Gaussian-fitting algorithm was applied to discriminate between two close foci (radius: 1 pixel, method: oval, iterations: 1000, minimal r^2 for optimization: 0.9). A tolerance distance of 0.3 µm outside the segmented cell boundary was set for maxima/foci association to parent cells. Analyzed images were manually inspected to confirm that the majority of cells were properly assigned. Shape descriptors, medial axis profiles, polarity, maxima/foci intensities and parent localization associations were recorded for each strain. Demographic representations of the fluorescence intensity of the 525/50 channel along the cell medial axis were performed for 500 randomized cells of each strain, sorted by cell length. Fluorescent signal at midcell was manually inspected. MicrobeJ analysis-derived data were collected from three independent sets of 500 randomized cells within datasets containing at least 2000 segmented cells for each strain. Alexa Fluor™ 488-labeled $FliC^{S267C}$ filaments were manually inspected in 500 randomized cells from sets of 8 images containing 100-200 segmented cells for each strain.

Statistical analysis

Statistical treatment of the data was performed using GraphPad Prism v8.3.0 software. Results are reported as the average and standard deviation of at least three biological replicates or image datasets, or median and interquartile interval for fluorescence foci quantification. Significance of the differences among strains was evaluated by means of the two-tailed Student's t-test for unpaired samples not assuming equal variance.

Bioinformatics analyses

Sequence alignmentes were performed using the MUSCLE package at the EMBL-EBI web site (https://www.ebi.ac.uk/Tools/msa/muscle/) (Edgar, 2004). Similarity between FimV/HubP proteins was scored using BLASTP at the National Center for Biotechnology Information web site (https://blast.ncbi.nlm.nih.gov/Blast.cgi) (Altschul *et al*., 1990).

RESULTS

FimV, FlhF and FleN are polarly located proteins that regulate flagellar function

The *P. putida* KT2440 ORF PP_1993 encodes an ortholog of *P. aeruginosa* FimV. *P. putida* FimV displays 55% identity and 68% similarity to its *P. aeruginosa* counterpart. To assess the possible involvement of FimV in flagellar assembly we constructed MRB97, a derivative of *P. putida* KT2442 (a spontaneous rifampicin-resistant mutant of the reference strain KT2440) bearing a complete deletion of PP_1993. KT2442-derived Δ*flhF*, Δ*fleN* and Δ*fleQ* mutants MRB69, MRB71 and MRB52 were previously described (Navarrete *et al*., 2019). The Δ*fimV*, Δ*flhF* and Δ*fleN* mutants displayed 39%-, 55%- and 71%-reduced motility halo diameter relative to the wild-type in a soft agar-based swimming assay **(Fig 1)**. The non-motile Δ*fleQ* mutant, used here as negative control, did not spread from the inoculation point. These results indicate that FimV, FlhF and FleN are not essential to flagellar motility, but are required for full flagellar function.

FimV controls FleN and FlhF association with the cell pole

The intracellular location of FimV, FlhF and FleN was assessed by expressing fluorescent GFP fusions from miniTn7 derivatives inserted in the chromosomes of the wild-type and mutant strains. A C-terminal FimV-GFP fusion and a N-terminal GFP-FleN fusion were produced from the salicylate-inducible P*sal* promoter. A C-terminal FlhF-GFP fusion was produced from its physiological P*flhF* promoter and translational start signals. Full complementation of the swimming defects of the cognate deletion mutants was observed with FlhF-GFP and uninduced FimV-GFP **(Supplemental Fig S1A and B)**. Salicylate-induced FimV-GFP synthesis was deleterious to the host strain and was henceforth omitted. Partial complementation was obtained with GFP-FleN both in the presence and in the absence of salicylate **(Supplemental Fig S1C)**, suggesting that the fusion protein only retains partial function. A C-terminal FleN-GFP fusion was also constructed and expressed, but it completely failed at complementation. Accordingly, we used the partially active N-terminal GFP-FleN fusion in this study.

All three fusion proteins formed fluorescent foci at the cell poles of the wild-type strain **(Fig 2A)**. FimV-GFP formed bipolar foci in the vast majority of cells and time-lapse fluorescence microscopy showed that FimV-GFP was recruited to the midcell region during cell division and remained permanently attached to the cell pole following daughter cell separation (**Fig 2B**). The distribution of the FimV-GFP foci was not substantially affected by the Δ*flhF* or Δ*fleN* mutations, nor was the distribution of FleN altered in the Δ*flhF* background **(Fig 2A)**. In contrast, GFP-FleN was distributed in the cytoplasm in the Δ*fimV* strain and polar foci were all but absent, indicating that FimV function is essential to polar targeting of FleN.

The polar distribution of FlhF-GFP was also deeply disturbed in the Δ*fimV* background **(Fig 2A)**. Visual inspection and quantitative analysis revealed a clear decrease in unipolar and bipolar FlhF-GFP distribution in the Δ*fimV* mutant resulting in a large proportion of vacant poles **(Fig 2A and 3A)**, accompanied by an increase in the frequency

of ectopic foci at non-polar locations **(Fig 3B)**. We hypothesized that FimV may contribute to FlhF recruitment to the new cell pole. To test this possibility, the dynamics of FlhF-GFP accumulation at the cell poles was monitored by time-lapse fluorescence microscopy **(Fig 3C and Supplemental videos SV1 and SV2)**. In the wild-type, FlhF-GFP foci were observed at the new cell pole shortly after cell division and remained at all poles for the duration of the experiment (i.e., 300 minutes). Deletion of *fimV* did not prevent FlhF-GFP recruitment to the new pole, but newly formed foci were stochastically disassembled (average lifespan of ~75 minutes) in the absence of FimV **(Fig 3C and Supplemental Fig S2)**. These results suggest that polar targeting of FlhF does not require FimV, but FimV promotes a stable association of FlhF with the cell poles. On the other hand, such permanent sequestration of FlhF may in turn prevent its association to the cell surface in non-polar locations.

FimV and FleN determine the timing of FlhF targeting to the new cell pole

Deletion of *fleN* resulted in a high frequency (>90%) of cells with polar FlhF-GFP foci, similarly to the wild-type. However, cells with a bipolar distribution were more prevalent in this background (79% bipolar and 15% unipolar *vs.* 58% and 34% in the wild-type) **(Fig 3A)**. In addition, a high incidence of cells bearing ectopic FlhF-GFP foci (62%) was also observed **(Fig 3B)**. As shown above **(Fig 3C)**, newly divided wild-type cells typically bear a single FlhF-GFP focus at the old pole. Eventually, a new focus emerges at the new pole and the resulting bipolar distribution remains unaltered until the following cell division. According to this model, we hypothesize that the higher frequency of bipolar FlhF-GFP distribution in the Δ*fleN* strain may be due to recruitment of the fluorescent protein to the new pole at an earlier stage of the cell cycle. To test this possibility, we used FlhF-GFP fluorescence demographic maps of length-sorted wild-type, Δ*fimV* and Δ*fleN* cells to assess the frequency of bipolar FlhF-GFP distribution in relation to cell length **(Supplemental Fig S3)**. The bipolar distribution frequency *vs.* cell length plots derived from the demographic maps (**Fig 4A**)

showed that the frequency of bipolarly distributed FlhF-GFP increases with cell length in the wild-type to reach a plateau of 80-90% in cells larger than ~3.5 μm, consistent with FlhF recruitment being followed by a stable association with the cell pole. In contrast, the frequency of bipolar distribution decreased with length from ~30% to ~15% in the Δ*fimV* mutant, as expected from the premature dissociation of FlhF-GFP observed in this background. The Δ*fleN* mutant replicated the correlation of bipolar distribution and cell length observed in the wild-type, but the frequency of bipolar distribution was greater at the shorter cells and the plateau was reached at ~3 μm, suggestive of premature polar recruitment of FlhF in this background.

The fluorescence demographic maps of length-sorted Δ*fimV* and Δ*fleN* cells also revealed visible accumulation of FlhF-GFP foci at midcell, particularly in longer cells (**Supplemental Fig S3**). This may be attributed to early FlhF recruitment to the emerging new cell pole during cell division, but before cytokinesis. Quantitative analysis of this phenomenon showed a low frequency of midcell FlhF-GFP (8%) in the wild-type strain that was increased 4-fold in the Δ*fimV* mutant and 3-fold in the Δ*fleN* mutant (**Fig 3B**). Midcell foci frequency *vs.* cell length plots (**Fig 3C**) revealed that midcell foci were restricted to cells longer than ~4 μm and their frequency increased with length in the wild-type strain. In the Δ*fimV* and Δ*fleN* mutants, accumulation of midcell FlhF-GFP foci was detected at shorter lengths (~3.5 μm) and their frequency was also greater. Taken together, these results suggest that FimV and FleN control the recruitment of FlhF to prevent its premature association to the new cell pole.

FleN limits FlhF association with the cell poles

We also examined the effect of FimV and FleN on the extent of FlhF-GFP association to the cell poles. Visual examination and fluorescence intensity quantification of the FlhF-GFP foci images revealed an increase in average polar foci intensity in the Δ*fleN* mutant **(Fig 2A and 4D)**, suggesting that FleN restricts polar accumulation of FlhF. A similar

increase was not observed in the Δ*fimV* mutant, indicating that FleN interaction with the cell poles is not required for this phenotype. Instead, polar FlhF-GFP foci intensity in the Δ*fimV* mutant was very low, likely reflecting the instability of FlhF association to the cell poles in this background.

We have previously shown that *P. putida* FleN acts as a negative regulator, antagonizing FleQ transcriptional activation of the Class II flagellar genes, including *flhF* (Leal-Morales *et al*., 2021). Higher FlhF levels may suffice to explain the increased association of FlhF-GFP to the cell poles in the Δ*fleN* strain, as well as the higher frequency of ectopic foci in this background **(Fig 3B)**. To assess the relevance of FleN-dependent transcriptional regulation to FlhF polar recruitment, we compared the effect of *fleN* deletion on FlhF-GFP accumulation when produced from a FleN-regulated or a FleN-independent promoter. To this end, we examined the location of FlhF-GFP in the Δ*flhF* and Δ*flhF-fleN* strains MRB71 and MRB78 expressing *flhF* from the P*flhF* or the P*sal* promoter in mini-Tn7 derivatives (**Fig 4E**). Quantification of the fluorescent foci at the cell poles confirmed that *fleN* deletion stimulates polar accumulation of FlhF-GFP produced from its natural, FleN-repressed promoter P*flhF* (**Fig 4F**). In the presence of FleN, polar FlhF-GFP fluorescence was higher when produced from P*sal*, and this effect was exacerbated in the presence of salicylate, suggesting that increased FlhF production is sufficient to stimulate its recruitment to the cell poles. Interestingly, fluorescence intensity was also greater in the absence of FleN when produced in a FleN-independent fashion from P*sal*, both in the presence and in the absence of salicylate. Taken together, these results suggest that FleN limits the polar accumulation of FlhF by downregulating *flhF* transcription and by a second, uncharacterized post-transcriptional mechanism.

FimV and FlhF determine the polar location of the flagellar proteins

A similar analysis was performed to determine the contribution of FimV, FlhF and FleN to the intracellular location of individual flagellar proteins. To this end, we engineered

FliF (MS-ring) and FliM (C-ring) protein fusions to GFPmut3, along with the FliC (filament) derivative FliC^{S267C}, bearing a serine-to-cysteine substitution to enable binding of fluorescent maleimide-derived fluorochromes. All three proteins were produced in mini-Tn*7* derivatives from their natural promoters (P*fliE*, P*fliL* and P*fliC*) and translational start signals and were shown to complement the null swimming phenotypes of the corresponding deletion mutants **(Supplemental Fig S4)**.

Analysis of FliF-GFP, FliM-GFP and FliC^{S267C} intracellular distribution in the wild-type strain revealed the presence of polar FliF-GFP and FliM-GFP foci and FliC^{S267C} filaments in >90% of the population (**Fig 5A and B**). Residual subpopulations of cells (<10%) displayed ectopic FliF-GFP or FliM-GFP foci in non-polar locations, while non-polar FliC^{S267C} filaments were not detected (**Fig 5C**). The Δ*flhF* mutant showed 29%- and 54%-decreased frequency of cells bearing polar FliF-GFP and FliM-GFP foci, respectively (**Fig 5A and B**), accompanied by large increase in the incidence of non-polar foci, present in 94% and 75% of the cells, respectively (**Fig. 5C**). In contrast, most Δ*flhF* cells lacked FliC^{S267C} filaments, with only 3% displaying polar filaments (**Fig. 5A and B**) and 12% ectopic filaments (**Fig. 5C**). Unlike *flhF*, deletion of *fimV* or *fleN* did not alter the overall frequency of cells bearing polar FliF-GFP or FliM-GFP foci or FliC^{S267C} filaments (**Fig. 4A and B**). However, ectopic FliF-GFP and FliM-GFP foci were also 5- to 10-fold more frequent in the Δ*fimV* and Δ*fleN* mutants (**Fig 4C**) while ectopic FliC^{S267C} filaments were found in less than 2% of the cells. We noticed that filaments formed in both polar and ectopic positions of the Δ*flhF* mutant cells were very short, often less than one wavelength, and not bundled in tufts **(Supplemental Fig S5)**, suggesting that FlhF is necessary for the completion of full-length flagella. Taken together, our results suggest that (i) FlhF restricts flagellar assembly to the cell poles; (ii) FlhF is not strictly required for assembly of the MS- and C-rings at polar or non-polar locations; (iii) FlhF is required for efficient filament assembly; and (iv) FimV and FleN prevent the accumulation of abortive flagellar assembly intermediates at ectopic sites.

FlhF is required for fT3SS activity and full Class III flagellar gene expression

The results above show that most Δ*flhF* cells bear FliF-GFP and FliM-GFP foci at polar or ectopic locations. In contrast, >85% Δ*flhF* cells were non-flagellated and FliC^{S267C} filaments, when present, were short and not bundled in tufts, suggesting a crucial role of FlhF in flagellar biogenesis beyond MS- and C-ring assembly. Since rod, hook and filament components (but not those of the MS- and C-rings) are secreted by way of the fT3SS, we speculated that flagellar secretion may be impaired in the absence of FlhF. In *E. coli* and other bacteria, the anti-σ factor FlgM is secreted to the medium *via* the fT3SS to release inhibition of its cognate σ factor FliA (Chevance & Hughes, 2008, Smith & Hoover, 2009), but this regulation has not been addressed in the genus *Pseudomonas*. To evaluate FlgM secretion and the possible involvement of FlhF, we produced a FlgM-FLAG fusion from P*sal* from a mini-Tn*7* derivative and detected it in cell fractions and culture supernatants by Western blot using an anti-FLAG antibody in the wild-type strain and the Δ*flhF* mutant (**Fig 6A**). An insertion mutant in *fliP*, an essential component of the fT3SS (henceforth designated the fT3SS$^-$ mutant) was used as a negative control. A band compatible with the molecular weight of FlgM-FLAG (~12 kDa) was detected in the cell fractions of the three strains and in the wild-type strain supernatant, but was conspicuously absent in those of the fT3SS$^-$ and Δ*flhF* mutants, indicating that FlgM is secreted by way of the flagella in *P. putida*, and FlhF is required for fT3SS function.

A simple prediction derived from the lack of FlgM secretion in the Δ*flhF* mutant is that FlgM will persist to inactivate FliA, leading to downregulation of the Class III promoters in this background. To test this hypothesis, we assessed the effect of *flhF* deletion on the expression of three Class III flagellar promoters: P*fliC*, P*cheA* and P*motA*, transcriptionally fused to *gfp-mut3* (Leal-Morales *et al*., 2021) (**Fig 6B**). Expression from all three promoters was high in the wild-type and decreased in the Δ*fliA* strain, as shown previously (Leal-Morales *et al*., 2021). All three promoters were also downregulated (5-, 3- and 2-fold,

respectively), in the Δ*flhF* mutant, suggesting that impaired FlgM secretion in the absence of FlhF precludes the release of FliA inactivation. Because FimV determines the stability of FlhF association to the cell poles, we also tested the activity of the three fusions in the Δ*fimV* strain. Deletion of *fimV* caused modest downregulation (<2-fold) of P*fliC*, and had no significant impact on P*cheA* and P*motA*, suggesting that transient association of FlhF with the cell poles is sufficient to support fT3SS assembly.

FleN prevents the polar accumulation of flagellar proteins

Our previous work showed that a *P. putida* Δ*fleN* mutant displays polar tufts with more flagella than the wild-type (Navarrete *et al*., 2019). This was also evident by visual inspection of the fluorescence microscopy images from cells producing FliC^{S267C} **(Fig 5A)**. Quantitative assessment of filament numbers from the images revealed a similar distribution, in which 3 or more filaments were found in roughly half of the cells, in the wild-type and Δ*fimV* strains **(Supplemental Fig S6)**. The vast majority (~95%) of flagellated Δ*flhF* cells displayed only 1-2 filaments. In contrast, more than three filaments were present in most (~75%) of the Δ*fleN* cells. Filament counting was not accurate for cells bearing more than three filaments. To test the impact of FleN on the accumulation of individual flagellar proteins, the intensity of the polar FliF-GFP and FliM-GFP foci was determined in the wild-type and Δ*fleN* strains **(Fig. 6C)**. Accurate quantification of fluorescence associated to the FliC^{S267C} filaments was not possible. As shown above for FlhF-GFP **(Fig 4D)**, FliF-GFP and FliM-GFP polar foci fluorescence was intensified in the absence of FleN. This result indicates that FleN prevents the accumulation of FlhF and flagellar intermediates at the cell pole. A similar increase in FliF and FliM protein foci fluorescence relative to the wild-type was not detected in the absence of FimV (**Fig 6C**), and visual assessment of the fluorescent label in the FliC^{S267C} filaments of the Δ*fimV* strain did not reveal substantial differences relative to the wild-type. As shown above for FlhF, these results suggest that inhibition of flagellar protein accumulation can occur in the absence of FleN association with the cell poles.

FimV and FleN regulate the timing of flagellar assembly

In bacteria bearing flagella at a single pole flagellar assembly follows a cycle in which postdivisional cells bear complete flagella at the old pole, and flagellar proteins are recruited *de novo* to the new pole during the cell cycle in an orderly fashion. As stated above, the frequency of cells bearing an individual flagellar protein at both poles is expected to mirror the time of recruitment of each individual flagellar protein. Accordingly, The frequency of bipolar distribution was 48%, 28% and 2% for FlhF-GFP, FliF-GFP and FliC^{S267C}, respectively **(Fig 5B)**. Along with the results shown above for FlhF, these results support an assembly hierarchy in which FlhF is targeted first, followed by FliF (MS-ring) and FliM (C-ring), with FliC (filament) only being recruited near the end of the cell cycle.

Deletion of *fimV* or *fleN* had a major impact on the polar distribution of the flagellar proteins. The Δ*fimV* mutant displayed increased bipolar distribution frequency of FliF-GFP (86%), FliM-GFP (64%) and FliC^{S267C} (10%) **(Fig 5B)**. On the other hand, *fleN* deletion boosted the frequency of bipolar distribution of FlhF-GFP (79%) and FliF-GFP (78%), but not FliC^{S267C} (1%). The bipolar distribution frequency *vs.* cell length plots derived from the demographic maps of length-sorted cells (**Supplemental Fig S7**) showed that flagellar proteins with increased bipolar distribution were targeted to the new pole at shorter cell lengths in the mutant backgrounds **(Fig 6D)**.

Visible midcell flagellar protein foci were also evident in longer cells (**Supplemental Fig S7**), as shown above for FlhF. Quantitative analysis of this phenomenon showed low frequencies of midcell FliF-GFP and FliM-GFP foci (4% and 1%, respectively) in the wild-type strain **(Fig 6E)**. The midcell FliF-GFP foci frequency was increased 4- and 3-fold in the Δ*fimV* and Δ*fleN* mutants, respectively. A modest increase (3- and 2-fold, respectively) was also observed with FliM-GFP. Midcell FliC^{S267C} filaments were not observed. Midcell foci frequency *vs.* cell length plots (**Fig 6F**) revealed that midcell FliF-GFP emerged at shorter cell lengths and occurred with increased frequency in longer cells of the mutant strains.

Although a similar trend was observed with FliM-GFP foci, the differences were small and the results inconclusive. Along with the observations for FlhF above, these results suggest that FimV and FleN prevent premature recruitment of the early flagellar components FlhF and FliF to the new cell poles that may even precede the completion of cell division.

DISCUSSION

Spatiotemporal and numerical control of flagellar assembly is a critical aspect of the regulation of motility in polarly flagellated bacteria (Kazmierczak & Hendrixson, 2013; Schuhmacher *et al*., 2015). Because of the asymmetry of their unipolar flagellation pattern, motile *P. putida* cells can only transmit their flagellar machinery to one of their offspring upon cell division. Hence, to secure motility of both daughter cells, *P. putida* must (i) identify the new pole as a site for flagella assembly, (ii) assemble *de novo* a tuft bearing the correct number of flagella (typically, three to six) at this site, and (iii) coordinate the timing of such assembly with the cell cycle to ensure emergence of the new flagella and motility of the daughter cell immediately after cell division. The work presented here identifies and characterizes the involvement of a novel element, the polar landmark protein FimV, and expands on the function of two previously described elements, FlhF and FleN (Navarrete *et al*., 2019), in the spatiotemporal and numerical control of flagellar assembly in *P. putida*. Our findings are summarized in **Fig 7**.

Three proteins, FimV, FlhF and FleN, are shown here to regulate the location, timing and number of flagella assembled during the cell cycle of *P. putida*. We have previously described that deletion of *flhF* or *fleN* led to defects in flagellar motility characterized by slower swimming and swarming in soft agar-based assays (Navarrete *et al*., 2019). Here we show that a Δ*fimV* mutant also displays clear motility defects (**Fig 1**). While the highly similar *P. aeruginosa* FimV protein regulates twitching motility (Carter *et al*., 2017), cAMP-mediated signaling (Inclan *et al*., 2016) and planktonic to biofilm transition (Nicastro *et al*., 2020; Bense *et al*., 2019; Schniederberend *et al*., 2019), it is not involved in flagellar function (Buensuceso

et al., 2017). FimV is part of the FimV/HubP/TspA protein family. Members of this family are highly variable in size and sequence but share a common architecture, with a N-terminal periplasmic domain featuring a peptidoglycan-binding LysM domain, followed by a transmembrane helix and a C-terminal cytoplasmic domain containing a variable number of tetratricopeptide repeat motifs (Buensuceso *et al*., 2016). However distantly related to FimV, HubP proteins have been shown to regulate flagellar assembly in *Vibrio cholerae*, *Shewanella putrefaciens*, *Vibrio alginolyticus*, *Vibrio vulnificus* and *Vibrio parahemolyticus* (Yamaichi *et al*., 2012**;** Rossmann *et al*., 2015; Takekawa *et al*., 2016; Park *et al*., 2019; Arroyo-Pérez & Ringgaard, 2021). Our results highlight the fact that members of the FimV/HubP/TspA family adopt specific roles that are adapted to the specific physiological needs of the host organism.

We have explored the function of FimV at the onset of *de novo* flagellar assembly in *P. putida*. FimV is targeted to the midcell region during cell division and remains permanently associated to the new poles formed after cytokinesis **(Fig 2)**. Recruitment of FimV to the midcell region is consistent with FimV-dependent recruitment of the type IVa pilus machinery to future cell division sites in *P. aeruginosa* (Carter *et al*., 2017) and the midcell localization of HubP in *V. cholerae* (Yamaichi *et al*., 2012) and *S. putrefaciens* (Rossmann *et al*., 2015), and may involve interaction of its periplasmic domain with septal peptidoglycan (Wehbi *et al*., 2011), or components of the cell division machinery (Galli *et al*., 2017).

FimV conditions the intracellular localization of the two known regulators of polar flagellar assembly in *P. putida*: FimV promotes polar targeting of FleN, and stabilizes FlhF association with the cell poles **(Figs 2A and 3C, Supplemental Figs S2 and S3 and Supplemental videos S1 and S2)**. In the absence of FimV, FleN shows a diffuse cytoplasmic location, while FlhF is associated to the cell surface at polar and non-polar positions **(Figs 2A and 3A)**, indicating that FlhF, but not FleN, may be intrinsically able of insertion in the cell membrane, as suggested for its *Vibrio* spp. counterparts (Kusumoto *et*

al., 2008; Green *et al*., 2009). The involvement of HubP in polar targeting of the FleN ortholog FlhG**,** has also been demonstrated in several *Vibrio* spp. (Yamaichi *et al*., 2012; Takekawa *et al*., 2016; Arroyo-Pérez & Ringgaard, 2021). Polar recruitment of FlhF in *P. putida* requires the participation of the membrane maintenance $TonB_m$-PocAB complex (Ainsaar *et al*., 2019), and a recent preprint proposed the involvement of FipA, an as of yet characterized protein of the *P. putida* flagellar cluster (Arroyo-Pérez *et al*., 2023 10.1101/2023.09.20.558563), but to the best of our knowledge this work remains unpublished. There are no precedents of members of the FimV/HubP/TspA family regulating the stability of the polar association of FlhF in any organism.

FlhF is an essential determinant of the polar location of the flagella in *P. putida*. The polar tuft of flagella displayed by the wild-type strain is paralleled by the strictly polar location of the flagellar proteins FliF, FliM and FliC, structural components of the MS-ring, C-ring and filament **(Fig 5)**. Such polar pattern of localization is obliterated in the Δ*flhF* mutant, where FliF and FliM nucleate at random polar and non-polar locations on the cell surface. FliF is a transmembrane protein and the main structural component of the MS ring, the earliest flagellar structure to be assembled and a molecular scaffold essential for the assembly of all the remaining flagellar components. FliM is a cytoplasmic protein with no membrane-binding domains, and its association with the growing flagellar structure is dependent on the previous assembly of the MS-ring and the incorporation of FliG, a second C-ring protein that interacts with both FliF and FliM (Macnab, 2003; Apel & Surette, 2008; Armitage & Berry 2020). The ability of the MS-ring to self-assemble and promote assembly of the C-ring has been previously described in *Salmonella* (Katayama *et al*., 1996; Kubori *et al*., 1997). Our results strongly suggest that FlhF acts primarily by luring FliF to assemble at the cell pole. Such recruitment serves a dual purpose: it directs specific assembly of the flagellar structure at the cell poles, and prevents flagellar assembly elsewhere.

In sharp contrast with the spontaneous FlhF-independent assembly of FliF- and FliM-containing flagellar structures, FliC-containing filaments are absent in the Δ*flhF* mutant, except for a small fraction of cells typically bearing one or two units **(Fig 5 and Supplemental Fig S5)**. A general inhibition of flagellation has been described in *flhF*-null mutants of *P. putida* (Pandza *et al*., 2000), and other bacterial species (Green *et al*., 2009; Kusumoto *et al*., 2008; Murray & Kazmierczak 2006; Balaban *et al*., 2009), but this phenomenon has not been investigated further. We hypothesized that flagellar assembly initiated in the absence of FlhF is most often hindered after FliM but before FliC addition, and then traced this defect to faulty secretion of the FliA-specific anti-σ factor FlgM **(Fig 6A)**. We propose that this is due to a failure in completion a functional fT3SS in the absence of FlhF, although the defect may also attributed to an inability to perform the secretion specificity switch that precedes export of the late flagellar secretion substrates, including FlgM (Ferris & Minamino, 2006). Consistent with its inability to evict FlgM from the cells, the Δ*flhF* mutant also displays reduced expression of at least three Class III (i.e., FliA-dependent) promoters **(Fig 6B)**. A negative effect of *flhF* deletion on late flagellar gene expression has been documented in *P. aeruginosa* (Murray & Kazmierczak, 2006), *V. cholerae* (Correa *et al*., 2005) *V. vulnificus* (Kim *et al*., 2012), *Campylobacter jejuni* (Ren *et al*., 2018; Li *et al*., 2022), *Helicobacter pylori* (Niehus *et al*., 2004), but the mechanisms behind this phenomenon have not been explored. We conclude that, in addition to its function in the determination of flagellar location, FlhF is necessary for efficient flagellar assembly beyond completion of the fT3SS. In addition, FlhF indirectly stimulates Class III transcription by enabling FlgM secretion.

Since FimV stabilizes the association of FlhF with the cell poles, we questioned whether the absence of FimV has any impact on any of the functions of FlhF. Polar flagellar assembly was to the best of our knowledge normal, as the Δ*fimV* mutant displayed polar tufts with flagellar numbers and morphology similar to the wild-type, indicating that transient

FlhF association with the cell pole is sufficient for polar recruitment and assembly of complete flagella **(Fig 5A and B)**. In contrast, the Δ*fimV* mutant displayed ectopic FliF- and FliM-containing assemblies that rarely led to filament completion **(Fig 5C)**, suggesting that permanent polar location of FlhF is necessary to prevent abortive flagellar assembly at ectopic positions.

FleN is a negative regulator that limits the number of flagella in *P. putida* (Navarrete *et al*., 2019) and other bacteria. Here we show that the increased number of flagella observed in thΔ*fleN* is mirrored by increased polar accumulation of FlhF, FliF, FliM and FliC (**Figs 2A, 4D, 5A, 6D and Supplemental Fig S6)** . We have previously described that FleN is an antagonist of FleQ activation of the Class II flagellar genes (Leal-Morales *et al*., 2022). Here we show that transcriptional downregulation of *flhF* transcription limits the polar accumulation of FlhF. However, we also show that FleN by way of a second, overlapping post-transcriptional mechanism **(Fig 4 E and F)**. In *B.subtilis*, FlhG stimulates the intrinsic GTPase activity of FlhF (Bange *et al*., 2011). Pole-bound FlhG is proposed to induce the detachment of FlhF from the cell pole by inducing the transition from an active, GTP bound dimer to an inactive, GDP-bound monomer (Schuhmacher *et al*., 2015). However, several lines of evidence suggest that this does not happen in *P. putida*. Firstly, we have shown that FlhF stays permanently bound to the cell pole in wild-type *P. putida*. Secondly, the *P. putida* Δ*fimV* mutant, which fails to recruit FleN to the cell pole, does not reproduce the hyperflagellation pattern of the Δ*fleN* mutant **(Fig 5A and Supplemental Fig S6)**, suggesting that FleN location at the cell pole is not essential to inhibition of flagellar assembly. Finally, the activator helix, a motif with the consensus DQAXXLR sequence present in the N-terminal domain of multiple FlhG proteins essential to stimulation of FlhF GTPase activity (Schuhmacher *et al*., 2015), is conspicuously absent in their *Pseudomonas* spp. counterparts **(Supplemental Fig S8)**. Since FleN represses all Class II flagellar promoters (Leal-Morales *et al*., 2022), transcriptional repression is also likely involved in the

control of structural flagellar protein accumulation. In addition, limited FlhF recruitment acts as a bottleneck to limit the number of flagella, and hence the accumulation of flagellar proteins. Because FimV is essential to polar recruitment of FleN, we questioned whether such polar location is required for FleN regulation of the polar accumulation of flagellar proteins. However, the Δ*fimV* mutant displays a number of polar flagella and amounts of flagellar proteins similar to the wild-type **(Fig 5A and Supplemental Fig S6)**, suggesting that the cytoplasmic form (or at best, both forms) of FleN is responsible for this regulatory function.

We have assigned a second, previously undescribed, role to FleN and FimV in determine the timing of the onset of flagellar assembly. FleN and FimV are necessary to prevent premature recruitment of FlhF and FliF **(Figs 4A and 6D and Supplemental Fig S7)**. In the absence of FleN or FimV, FlhF and FliF are found to accumulate at midcell in predivisional cells **(Figs 4B and C and 6E and F and Supplemental Fig S7)**, suggesting that targeting may occur even before completion of the previous cell division. Because FimV recruits FleN to the cell pole, we are inclined to believe that polar location of FleN is essential to this function. FimV on the other hand may or may not play an additional role other than facilitate the polar location of FleN. We are not aware of previous studies connecting FimV or FleN function to the time of flagellar assembly. The biological relevance of the correct timing in the initiation of flagellar is as of now unclear and will be a subject of further investigation in the near future.

ACKNOWLEDGMENTS

We wish to thank Enrique Flores, Antonia Herrero, Carmen Beuzón and Javier Ruiz-Albert for thoghtful advice and discussion. This work was funded by grants PGC2018-097151- B-100 and PID2021-126121N B-I00 of the Spanish Ministerio de Ciencia e Innovación, and by predoctoral FPU contract 19/02899 of the Spanish Ministerio de Educación y Formación Profesional, awarded to M P-S.

REFERENCES

1. Ainsaar K, Tamman H, Kasvandik S, Tenson T, Hõrak R. The TonB$_m$-PocAB System Is Required for Maintenance of Membrane Integrity and Polar Position of Flagella in Pseudomonas putida. J Bacteriol. 2019 Aug 8;201(17):e00303-19. doi: 10.1128/JB.00303-19. PMID: 31182498; PMCID: PMC6689306.
2. Altschul SF, Gish W, Miller W, Myers EW, Lipman DJ. Basic local alignment search tool. J Mol Biol. 1990 Oct 5;215(3):403-10. doi: 10.1016/S0022-2836(05)80360-2. PMID: 2231712.
3. Altegoer F, Schuhmacher J, Pausch P, Bange G. From molecular evolution to biobricks and synthetic modules: a lesson by the bacterial flagellum. Biotechnol Genet Eng Rev. 2014 Oct;30(1-2):49-64. doi: 10.1080/02648725.2014.921500. PMID: 25023462.
4. Altinoglu I, Abriat G, Carreaux A, Torres-Sánchez L, Poidevin M, Krasteva PV, Yamaichi Y. Analysis of HubP-dependent cell pole protein targeting in Vibrio cholerae uncovers novel motility regulators. PLoS Genet. 2022 Jan 12;18(1):e1009991. doi: 10.1371/journal.pgen.1009991. Erratum in: PLoS Genet. 2022 Mar 1;18(3):e1010094. PMID: 35020734; PMCID: PMC8789113.
5. Amako K, Umeda A. Flagellation of Pseudomonas aeruginosa during the cell division cycle. Microbiol Immunol. 1982;26(2):113-7. doi: 10.1111/j.1348-0421.1982.tb00160.x. PMID: 6806572.
6. Apel D, Surette MG. Bringing order to a complex molecular machine: the assembly of the bacterial flagella. Biochim Biophys Acta. 2008 Sep;1778(9):1851-8. doi: 10.1016/j.bbamem.2007.07.005. Epub 2007 Jul 24. PMID: 17719558.
7. Armitage JP, Berry RM. Assembly and Dynamics of the Bacterial Flagellum. Annu Rev Microbiol. 2020 Sep 8;74:181-200. doi: 10.1146/annurev-micro-090816-093411. Epub 2020 Jun 30. PMID: 32603624.

8. Arroyo-Pérez EE, Ringgaard S. Interdependent Polar Localization of FlhF and FlhG and Their Importance for Flagellum Formation of *Vibrio parahaemolyticus*. Front Microbiol. 2021 Mar 17;12:655239. doi: 10.3389/fmicb.2021.655239. PMID: 33815347; PMCID: PMC8009987.

9. Balaban M, Joslin SN, Hendrixson DR. FlhF and its GTPase activity are required for distinct processes in flagellar gene regulation and biosynthesis in Campylobacter jejuni. J Bacteriol. 2009 Nov;191(21):6602-11. doi: 10.1128/JB.00884-09. Epub 2009 Aug 28. PMID: 19717591; PMCID: PMC2795303.

10. Bange G, Kümmerer N, Grudnik P, Lindner R, Petzold G, Kressler D, Hurt E, Wild K, Sinning I. Structural basis for the molecular evolution of SRP-GTPase activation by protein. Nat Struct Mol Biol. 2011 Nov 6;18(12):1376-80. doi: 10.1038/nsmb.2141. PMID: 22056770.

11. Bense S, Bruchmann S, Steffen A, Stradal TEB, Häussler S, Düvel J. Spatiotemporal control of FlgZ activity impacts Pseudomonas aeruginosa flagellar motility. Mol Microbiol. 2019 Jun;111(6):1544-1557. doi: 10.1111/mmi.14236. Epub 2019 Mar 29. PMID: 30864240.

12. Buensuceso RN, Nguyen Y, Zhang K, Daniel-Ivad M, Sugiman-Marangos SN, Fleetwood AD, Zhulin IB, Junop MS, Howell PL, Burrows LL. The Conserved Tetratricopeptide Repeat-Containing C-Terminal Domain of Pseudomonas aeruginosa FimV Is Required for Its Cyclic AMP-Dependent and -Independent Functions. J Bacteriol. 2016 Jul 28;198(16):2263-74. doi: 10.1128/JB.00322-16. PMID: 27297880; PMCID: PMC4966435.

13. Buensuceso RNC, Daniel-Ivad M, Kilmury SLN, Leighton TL, Harvey H, Howell PL, Burrows LL. Cyclic AMP-Independent Control of Twitching Motility in Pseudomonas aeruginosa. J Bacteriol. 2017 Jul 25;199(16):e00188-17. doi: 10.1128/JB.00188-17. PMID: 28583947; PMCID: PMC5527385.

14. Carter T, Buensuceso RN, Tammam S, Lamers RP, Harvey H, Howell PL, Burrows LL. The Type IVa Pilus Machinery Is Recruited to Sites of Future Cell Division. mBio. 2017 Jan 31;8(1):e02103-16. doi: 10.1128/mBio.02103-16. PMID: 28143978; PMCID: PMC5285504.

15. Correa NE, Peng F, Klose KE. Roles of the regulatory proteins FlhF and FlhG in the Vibrio cholerae flagellar transcription hierarchy. J Bacteriol. 2005 Sep;187(18):6324-32. doi: 10.1128/JB.187.18.6324-6332.2005. PMID: 16159765; PMCID: PMC1236648.

16. Chevance FF, Hughes KT. Coordinating assembly of a bacterial macromolecular machine. Nat Rev Microbiol. 2008 Jun;6(6):455-65. doi: 10.1038/nrmicro1887. PMID: 18483484; PMCID: PMC5963726.

17. Choi KH, Gaynor JB, White KG, Lopez C, Bosio CM, Karkhoff-Schweizer RR, Schweizer HP. A Tn7-based broad-range bacterial cloning and expression system. Nat Methods. 2005 Jun;2(6):443-8. doi: 10.1038/nmeth765. PMID: 15908923.

18. Choi KH, Kumar A, Schweizer HP. A 10-min method for preparation of highly electrocompetent Pseudomonas aeruginosa cells: application for DNA fragment transfer between chromosomes and plasmid transformation. J Microbiol Methods. 2006 Mar;64(3):391-7. doi: 10.1016/j.mimet.2005.06.001. Epub 2005 Jun 28. PMID: 15987659.

19. Dos Santos VA, Heim S, Moore ER, Strätz M, Timmis KN. Insights into the genomic basis of niche specificity of Pseudomonas putida KT2440. Environ Microbiol. 2004 Dec;6(12):1264-86. doi: 10.1111/j.1462-2920.2004.00734.x. PMID: 15560824.

20. Ducret A, Quardokus EM, Brun YV. MicrobeJ, a tool for high throughput bacterial cell detection and quantitative analysis. Nat Microbiol. 2016 Jun 20;1(7):16077. doi: 10.1038/nmicrobiol.2016.77. PMID: 27572972; PMCID: PMC5010025.

21. Edgar RC. MUSCLE: multiple sequence alignment with high accuracy and high throughput. Nucleic Acids Res. 2004 Mar 19;32(5):1792-7. doi: 10.1093/nar/gkh340. PMID: 15034147; PMCID: PMC390337.

22. Espinosa-Urgel M, Salido A, Ramos J-L. Genetic analysis of functions involved in adhesion of Pseudomonas putida to seeds. J Bacteriol. 2000;182: 2363–2369. 10.1128/JB.182.9.2363-2369.2000

23. Ferris HU, Minamino T. Flipping the switch: bringing order to flagellar assembly. Trends Microbiol. 2006 Dec;14(12):519-26. doi: 10.1016/j.tim.2006.10.006. Epub 2006 Oct 25. PMID: 17067800.

24. Galli E, Paly E, Barre FX. Late assembly of the Vibrio cholerae cell division machinery postpones septation to the last 10% of the cell cycle. Sci Rep. 2017 Mar 16;7:44505. doi: 10.1038/srep44505. PMID: 28300142; PMCID: PMC5353653.

25. Gibson DG. Enzymatic assembly of overlapping DNA fragments. Methods Enzymol. 2011;498:349-61. doi: 10.1016/B978-0-12-385120-8.00015-2. PMID: 21601685; PMCID: PMC7149801.

26. Green JC, Kahramanoglou C, Rahman A, Pender AM, Charbonnel N, Fraser GM. Recruitment of the earliest component of the bacterial flagellum to the old cell division pole by a membrane-associated signal recognition particle family GTP-binding protein. J Mol Biol. 2009 Aug 28;391(4):679-90. doi: 10.1016/j.jmb.2009.05.075. Epub 2009 Jun 1. PMID: 19497327.

27. Hintsche M, Waljor V, Großmann R, Kühn MJ, Thormann KM, Peruani F, Beta C. A polar bundle of flagella can drive bacterial swimming by pushing, pulling, or coiling around the cell body. Sci Rep. 2017 Dec 1;7(1):16771. doi: 10.1038/s41598-017-16428-9. Erratum in: Sci Rep. 2022 Aug 12;12(1):13732. PMID: 29196650; PMCID: PMC5711944.

28. Inclan YF, Persat A, Greninger A, Von Dollen J, Johnson J, Krogan N, Gitai Z, Engel JN. A scaffold protein connects type IV pili with the Chp chemosensory system to mediate activation of virulence signaling in Pseudomonas aeruginosa. Mol Microbiol. 2016 Aug;101(4):590-605. doi: 10.1111/mmi.13410. Epub 2016 May 27. PMID: 27145134; PMCID: PMC4980298.

29. Inoue H, Nojima H, Okayama H. High efficiency transformation of Escherichia coli with plasmids. Gene. 1990 Nov 30;96(1):23-8. doi: 10.1016/0378-1119(90)90336-p. PMID: 2265755.

30. Katayama E, Shiraishi T, Oosawa K, Baba N, Aizawa S. Geometry of the flagellar motor in the cytoplasmic membrane of Salmonella typhimurium as determined by stereo-photogrammetry of quick-freeze deep-etch replica images. J Mol Biol. 1996 Jan 26;255(3):458-75. doi: 10.1006/jmbi.1996.0038. PMID: 8568890.

31. Kazmierczak BI, Hendrixson DR. Spatial and numerical regulation of flagellar biosynthesis in polarly flagellated bacteria. Mol Microbiol. 2013 May;88(4):655-63. doi: 10.1111/mmi.12221. Epub 2013 Apr 21. PMID: 23600726; PMCID: PMC3654036.

32. Kim SM, Lee DH, Choi SH. Evidence that the Vibrio vulnificus flagellar regulator FlhF is regulated by a quorum sensing master regulator SmcR. Microbiology (Reading). 2012 Aug;158(Pt 8):2017-2025. doi: 10.1099/mic.0.059071-0. Epub 2012 Jun 7. PMID: 22679105.

33. Kubori T, Yamaguchi S, Aizawa S. Assembly of the switch complex onto the MS ring complex of Salmonella typhimurium does not require any other flagellar proteins. J Bacteriol. 1997 Feb;179(3):813-7. doi: 10.1128/jb.179.3.813-817.1997. PMID: 9006037; PMCID: PMC178764.

34. Kusumoto A, Shinohara A, Terashima H, Kojima S, Yakushi T, Homma M. Collaboration of FlhF and FlhG to regulate polar-flagella number and localization in Vibrio

alginolyticus. Microbiology (Reading). 2008 May;154(Pt 5):1390-1399. doi: 10.1099/mic.0.2007/012641-0. PMID: 18451048.

35. Leal-Morales A, Pulido-Sánchez M, López-Sánchez A, Govantes F. Transcriptional organization and regulation of the Pseudomonas putida flagellar system. Environ Microbiol. 2022 Jan;24(1):137-157. doi: 10.1111/1462-2920.15857. Epub 2021 Dec 2. PMID: 34859548.

36. Leifson E. Staining, shape and arrangement of bacterial flagella. J Bacteriol. 1951 Oct;62(4):377-89. doi: 10.1128/jb.62.4.377-389.1951. PMID: 14897809; PMCID: PMC386144.

37. Li X, Chai Q, Zheng L, Huang P, Gundogdu O, Jiao X, Tang Y, Huang J. Investigating the role of BN-domains of FlhF involved in flagellar synthesis in Campylobacter jejuni. Microbiol Res. 2022 Mar;256:126944. doi: 10.1016/j.micres.2021.126944. Epub 2021 Dec 14. PMID: 34952396.

38. Macnab R M. Flagella and motility. In: Neidhardt F C, Curtiss III R, Ingraham J L, Lin E C C, Low K B, Magasanik B, Reznikoff W S, Riley M, Schaechter M, Umbarger H E, editors. *Escherichia coli* and *Salmonella*: cellular and molecular biology. 2nd ed. Washington, D.C: ASM Press; 1996. pp. 123–145

39. Macnab RM. How bacteria assemble flagella. Annu Rev Microbiol. 2003;57:77-100. doi: 10.1146/annurev.micro.57.030502.090832. Epub 2003 May 1. PMID: 12730325.

40. Martínez-García E, Nikel PI, Chavarría M, de Lorenzo V. The metabolic cost of flagellar motion in Pseudomonas putida KT2440. Environ Microbiol. 2014 Jan;16(1):291-303. doi: 10.1111/1462-2920.12309. Epub 2013 Nov 18. PMID: 24148021.

41. Matilla MA, Krell T. Chemoreceptor-based signal sensing. Curr Opin Biotechnol. 2017 Jun;45:8-14. doi: 10.1016/j.copbio.2016.11.021. Epub 2017 Jan 11. PMID: 28088095.

42. Murray TS, Kazmierczak BI. FlhF is required for swimming and swarming in Pseudomonas aeruginosa. J Bacteriol. 2006 Oct;188(19):6995-7004. doi: 10.1128/JB.00790-06. PMID: 16980502; PMCID: PMC1595508.

43. Navarrete B, Leal-Morales A, Serrano-Ron L, Sarrió M, Jiménez-Fernández A, Jiménez-Díaz L, López-Sánchez A, Govantes F. Transcriptional organization, regulation and functional analysis of flhF and fleN in Pseudomonas putida. PLoS One. 2019 Mar 19;14(3):e0214166. doi: 10.1371/journal.pone.0214166. PMID: 30889223; PMCID: PMC6424431.

44. Nicastro GG, Kaihami GH, Pulschen AA, Hernandez-Montelongo J, Boechat AL, de Oliveira Pereira T, Rosa CGT, Stefanello E, Colepicolo P, Bordi C, Baldini RL. c-di-GMP-related phenotypes are modulated by the interaction between a diguanylate cyclase and a polar hub protein. Sci Rep. 2020 Feb 20;10(1):3077. doi: 10.1038/s41598-020-59536-9. PMID: 32080219; PMCID: PMC7033161.

45. Niehus E, Gressmann H, Ye F, Schlapbach R, Dehio M, Dehio C, Stack A, Meyer TF, Suerbaum S, Josenhans C. Genome-wide analysis of transcriptional hierarchy and feedback regulation in the flagellar system of Helicobacter pylori. Mol Microbiol. 2004 May;52(4):947-61. doi: 10.1111/j.1365-2958.2004.04006.x. PMID: 15130117.

46. Pandza S, Baetens M, Park CH, Au T, Keyhan M, Matin A. The G-protein FlhF has a role in polar flagellar placement and general stress response induction in Pseudomonas putida. Mol Microbiol. 2000 Apr;36(2):414-23. doi: 10.1046/j.1365-2958.2000.01859.x. PMID: 10792727.

47. Park S, Yoon J, Lee CR, Lee JY, Kim YR, Jang KS, Lee KH, Seok YJ. Polar landmark protein HubP recruits flagella assembly protein FapA under glucose limitation in Vibrio vulnificus. Mol Microbiol. 2019 Jul;112(1):266-279. doi: 10.1111/mmi.14268. Epub 2019 May 18. PMID: 31058375.

48. Parkinson JS. cheA, cheB, and cheC genes of Escherichia coli and their role in chemotaxis. J Bacteriol. 1976 May;126(2):758-70. doi: 10.1128/jb.126.2.758-770.1976. PMID: 770453; PMCID: PMC233211.

49. Ren F, Lei T, Song Z, Yu T, Li Q, Huang J, Jiao XA. Could FlhF be a key element that controls Campylobacter jejuni flagella biosynthesis in the initial assembly stage? Microbiol Res. 2018 Mar;207:240-248. doi: 10.1016/j.micres.2017.12.006. Epub 2017 Dec 19. PMID: 29458860.

50. Rick T, Kreiling V, Höing A, Fiedler S, Glatter T, Steinchen W, Hochberg G, Bähre H, Seifert R, Bange G, Knauer SK, Graumann PL, Thormann KM. GGDEF domain as spatial on-switch for a phosphodiesterase by interaction with landmark protein HubP. NPJ Biofilms Microbiomes. 2022 May 2;8(1):35. doi: 10.1038/s41522-022-00297-w. PMID: 35501424; PMCID: PMC9061725.

51. Rodríguez-Herva JJ, Duque E, Molina-Henares MA, Navarro-Avilés G, Van Dillewijn P, De La Torre J, Molina-Henares AJ, La Campa AS, Ran FA, Segura A, Shingler V, Ramos JL. Physiological and transcriptomic characterization of a fliA mutant of Pseudomonas putida KT2440. Environ Microbiol Rep. 2010 Jun;2(3):373-80. doi: 10.1111/j.1758-2229.2009.00084.x. Epub 2009 Oct 7. PMID: 23766109.

52. Rossmann F, Brenzinger S, Knauer C, Dörrich AK, Bubendorfer S, Ruppert U, Bange G, Thormann KM. The role of FlhF and HubP as polar landmark proteins in Shewanella putrefaciens CN-32. Mol Microbiol. 2015 Nov;98(4):727-42. doi: 10.1111/mmi.13152. Epub 2015 Sep 10. PMID: 26235439.

53. Sambrook, JE and Russell, DW. Molecular Cloning, a Laboratory Manual. 2000. Cold Spring Harbor, New York, USA: Cold Spring Harbor Laboratory Press

54. Schneider CA, Rasband WS, Eliceiri KW. NIH Image to ImageJ: 25 years of image analysis. Nat Methods. 2012 Jul;9(7):671-5. doi: 10.1038/nmeth.2089. PMID: 22930834; PMCID: PMC5554542.

55. Schniederberend M, Williams JF, Shine E, Shen C, Jain R, Emonet T, Kazmierczak BI. Modulation of flagellar rotation in surface-attached bacteria: A pathway for rapid surface-sensing after flagellar attachment. PLoS Pathog. 2019 Nov 4;15(11):e1008149. doi: 10.1371/journal.ppat.1008149. PMID: 31682637; PMCID: PMC6855561.

56. Schuhmacher JS, Thormann KM, Bange G. How bacteria maintain location and number of flagella? FEMS Microbiol Rev. 2015 Nov;39(6):812-22. doi: 10.1093/femsre/fuv034. Epub 2015 Jul 20. PMID: 26195616.

57. Smith TG, Hoover TR. Deciphering bacterial flagellar gene regulatory networks in the genomic era. Adv Appl Microbiol. 2009;67:257-95. doi: 10.1016/S0065-2164(08)01008-3. PMID: 19245942.

58. Takekawa N, Kwon S, Nishioka N, Kojima S, Homma M. HubP, a Polar Landmark Protein, Regulates Flagellar Number by Assisting in the Proper Polar Localization of FlhG in Vibrio alginolyticus. J Bacteriol. 2016 Oct 21;198(22):3091-3098. doi: 10.1128/JB.00462-16. PMID: 27573015; PMCID: PMC5075038.

59. Terashima H, Kojima S, Homma M. Flagellar motility in bacteria structure and function of flagellar motor. Int Rev Cell Mol Biol. 2008;270:39-85. doi: 10.1016/S1937-6448(08)01402-0. PMID: 19081534.

60. Wehbi H, Portillo E, Harvey H, Shimkoff AE, Scheurwater EM, Howell PL, Burrows LL. The peptidoglycan-binding protein FimV promotes assembly of the Pseudomonas aeruginosa type IV pilus secretin. J Bacteriol. 2011 Jan;193(2):540-50. doi: 10.1128/JB.01048-10. Epub 2010 Nov 19. PMID: 21097635; PMCID: PMC3019827.

61. Yamaichi Y, Bruckner R, Ringgaard S, Möll A, Cameron DE, Briegel A, Jensen GJ, Davis BM, Waldor MK. A multidomain hub anchors the chromosome segregation and chemotactic machinery to the bacterial pole. Genes Dev. 2012 Oct 15;26(20):2348-60. doi: 10.1101/gad.199869.112. PMID: 23070816; PMCID: PMC3475806.

FIGURES

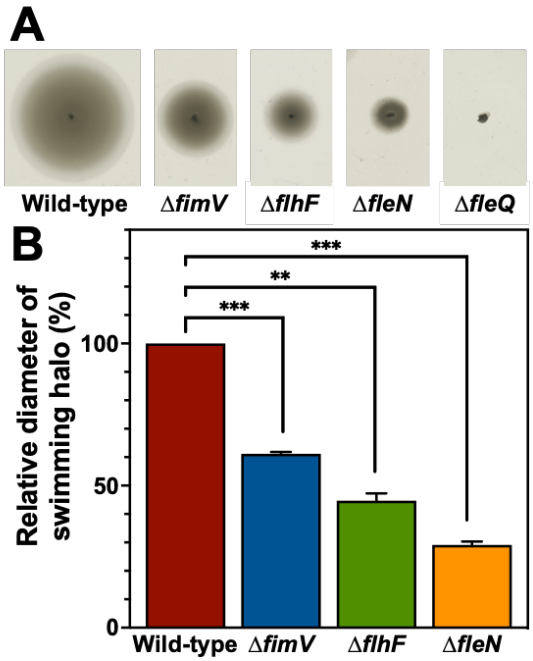

Figure 1. Soft agar-based swimming motility assay of the Δ*fimV*, Δ*flhF* and Δ*fleN* mutants. A. Images of the **s**wimming halos. **B.** Motility halo diameters. Columns and error bars represent average and standard deviation of at least three separate replicates. Values are relative to the wild-type strain (100%). Stars denote *p*-values of the two-tailed Student's T test not assuming equal variance (*=$p<0.05$; **= $p<0.01$; ***= $p<0.001$; ****= $p<0.0001$).

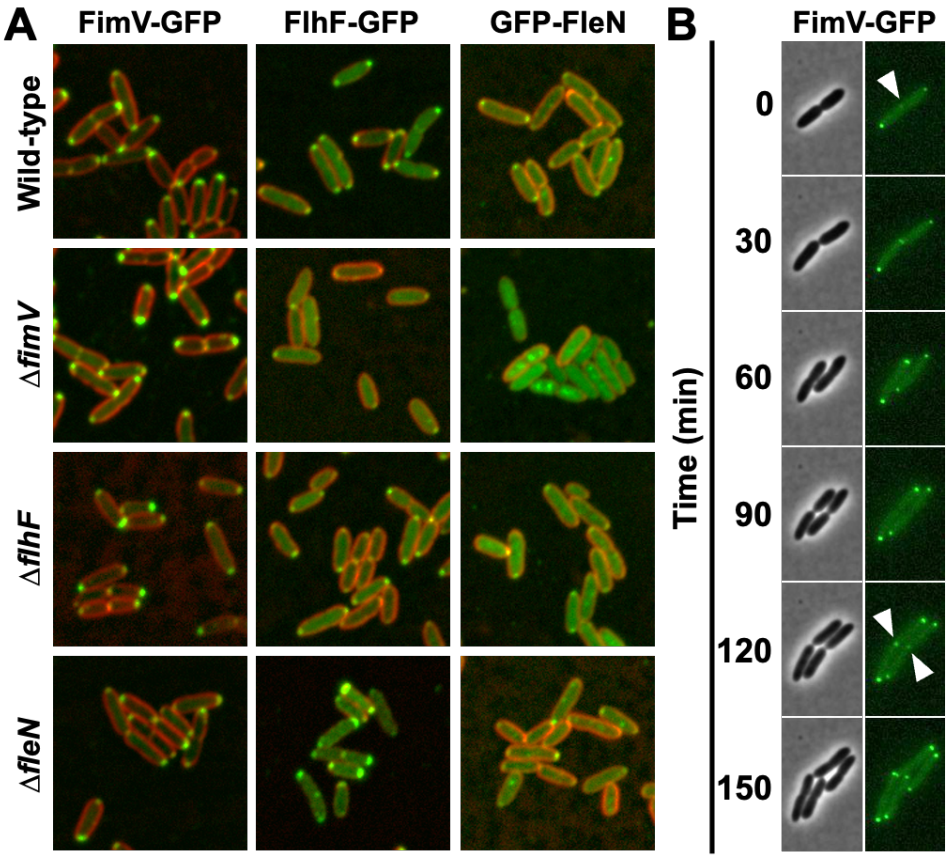

Figure 2. Intracellular location of regulatory proteins of flagellar assembly. A. Fluorescence images of wild-type, Δ*fimV*, Δ*flhF* and Δ*fleN* cells expressing FimV-GFP, FlhF-GFP or GFP-FleN. FM^{TM} 4-64 was used as membrane stain (red). **B.** Time-lapse images of wild-type cells expressing FimV-GFP. Bright field (left) and fluorescence (right). Arrowheads indicate fluorescent foci emerging during cell division.

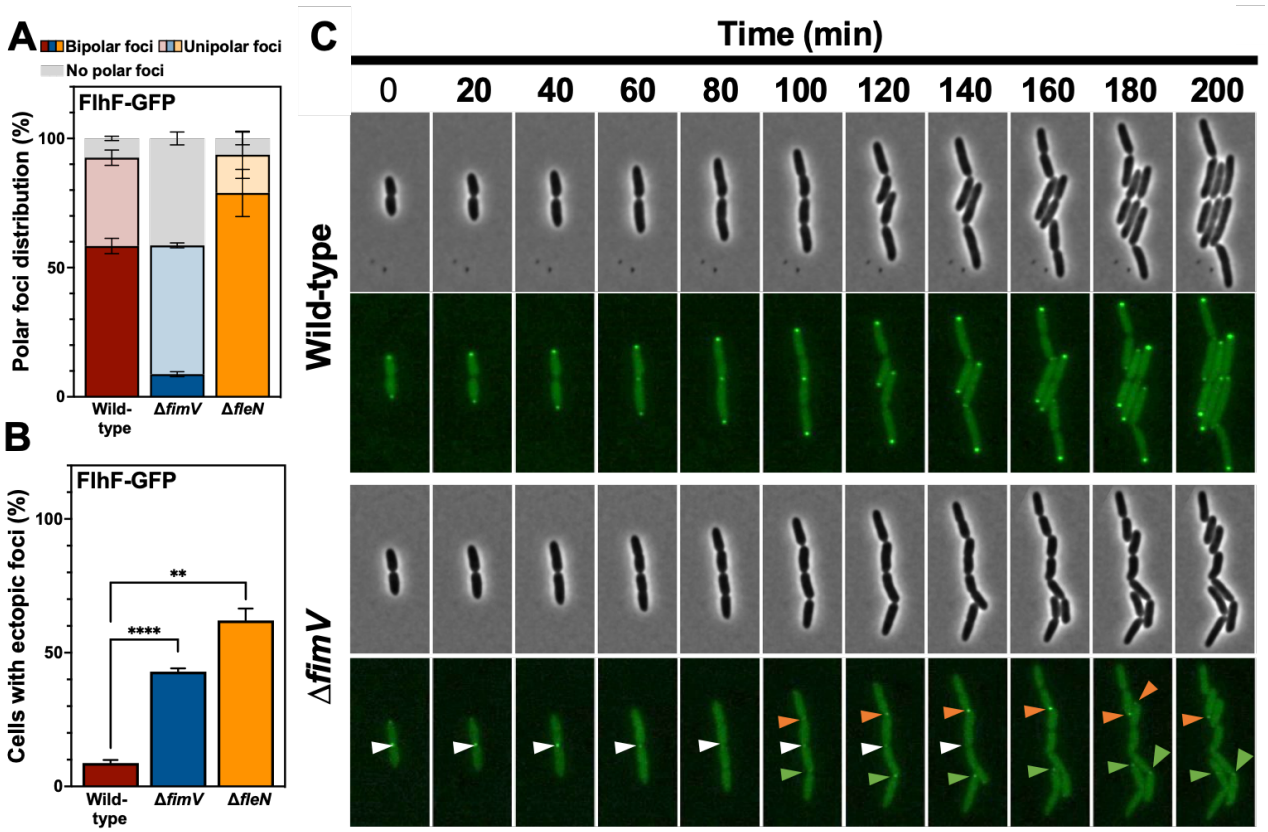

Figure 3. Analysis of intracellular FlhF-GFP location. A. Frequency of wild-type, Δ*fimV* and Δ*fleN* cells bearing bipolar, unipolar or no polar FlhF-GFP foci. **B.** Frequency of wild-type, Δ*fimV* and Δ*fleN* cells bearing ectopic FlhF-GFP foci. Columns and error bars represent average and standard deviation of at least three separate replicates (n=500 cells). Stars denote *p*-values of the two-tailed Student's T test not assuming equal variance (*=$p<0.05$; **= $p<0.01$; ***= $p<0.001$; ****= $p<0.0001$). **C.** Time-lapse images of wild-type (top two rows) and Δ*fimV* (bottom two rows) cells expressing FlhF-GFP. Bright field (first and third rows) and fluorescence (second and fourth rows). Arrowheads indicate three separate fluorescent foci.

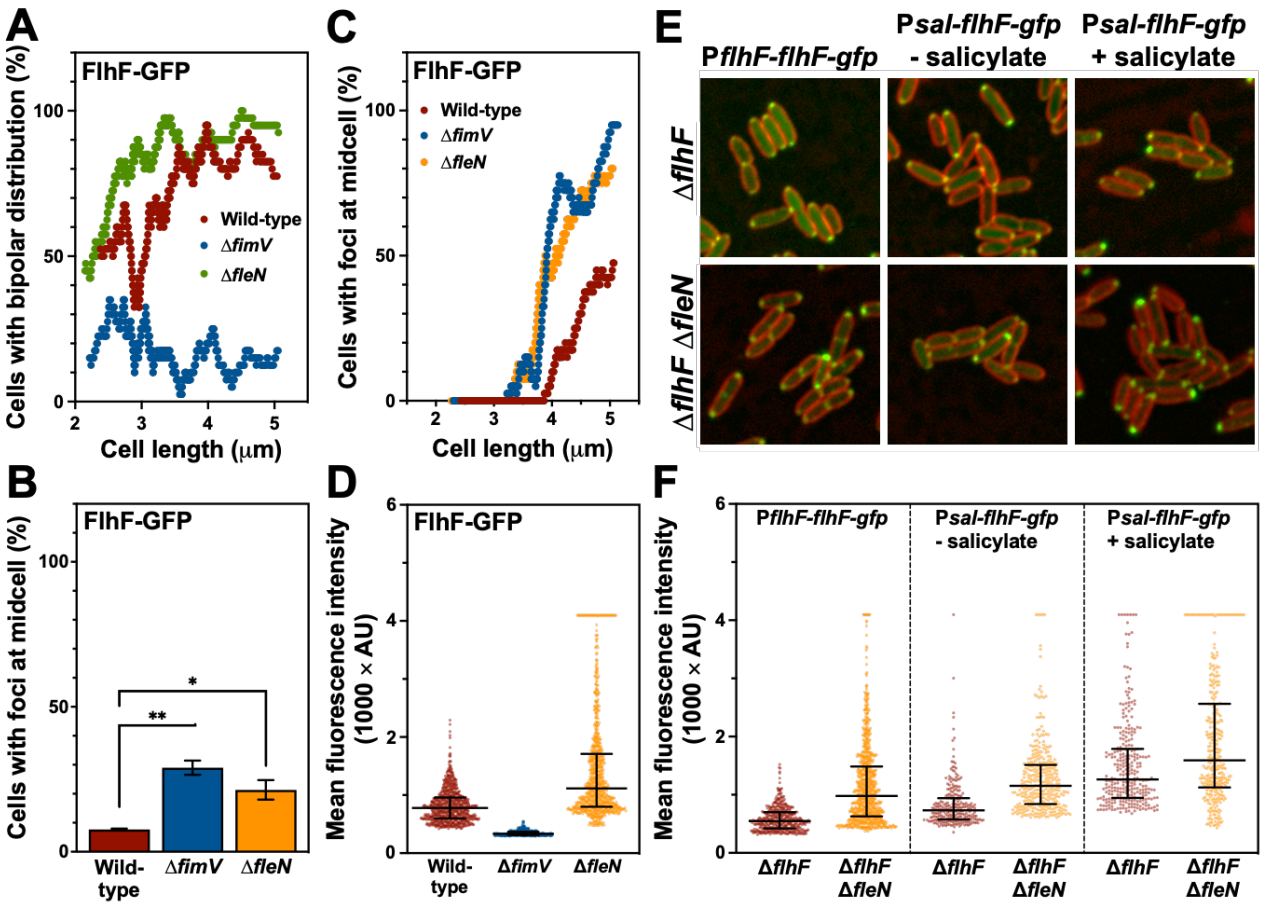

Figure 4. Analysis of intracellular FlhF-GFP location and foci intensity. A and C. Frequency of wild-type, Δ*fimV* and Δ*fleN* cells displaying bipolar FlhF-GFP distribution (**A**) or midcell foci (**C**) *vs*. cell length. Foci were scored from a set of 500 length-sorted cells of each strain in consecutive 40-cell windows and the frequency was plotted against the average length of each 40-cell set. **B.** Frequency of midcell FlhF-GFP foci in wild-type, Δ*fimV* and Δ*fleN* cells. Columns and error bars represent average and standard deviation of at least three separate replicates (n=500 cells). Stars denote *p*-values of the two-tailed Student's T test not assuming equal variance (*=$p<0.05$; **= $p<0.01$; ***= $p<0.001$; ****= $p<0.0001$). **D and F.** Mean fluorescence intensity of polar FlhF-GFP foci in (**D**) wild-type, Δ*fimV* or Δ*fleN* cells bearing P*flhF-flhF-gfp*, or (**F**) Δ*flhF or* Δ*flhF* Δ*fleN* cells bearing P*flhF-flhF-gfp* (left) or P*sal-flhF-gfp* in the absence (center) or in the presence (right) of 2 mM salicylate. Points correspond to individual fluorescence intensity values, bars denote the median and the interquartile interval of the distribution. **E.** Fluorescence microscopy images of Δ*flhF* (top) *or* Δ*flhF*Δ*fleN* (bottom) cells bearing P*flhF-flhF-gfp* (left) or P*sal-flhF-gfp* in the absence (center) or in the presence (right) of 2 mM salicylate. FM™ 4-64 was used as membrane stain (red).

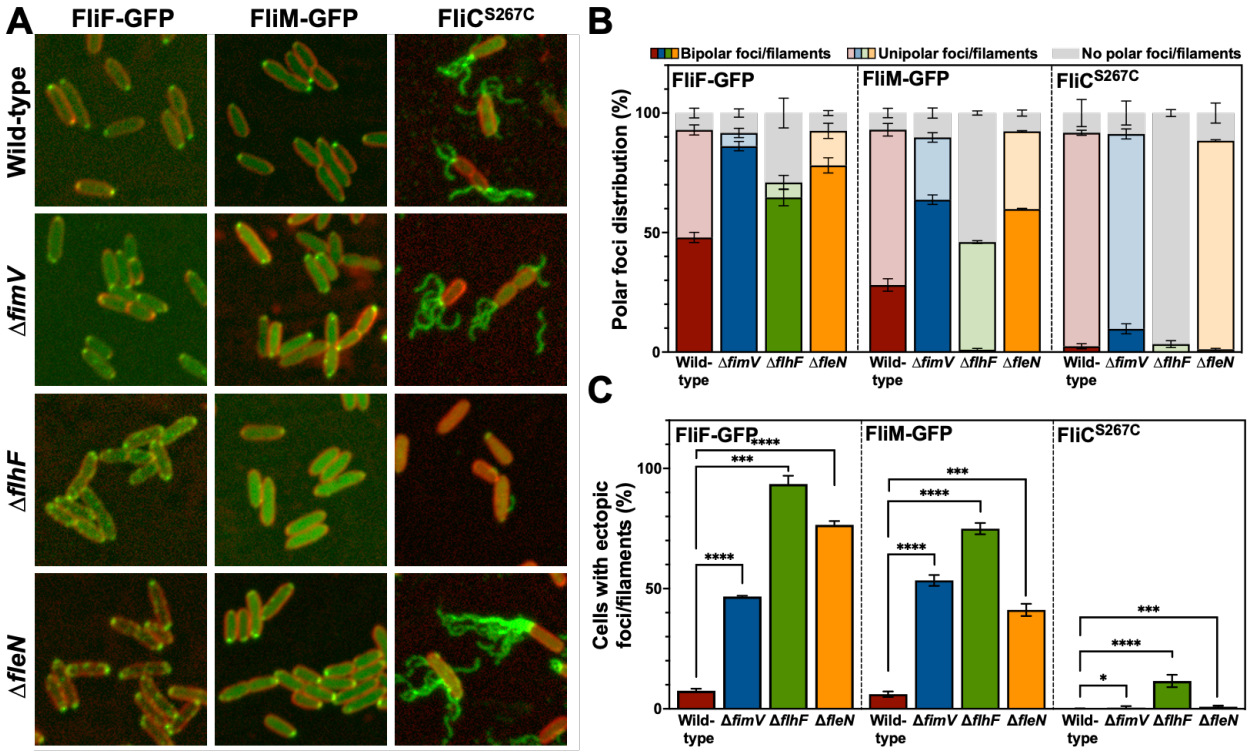

Figure 5. Intracellular location of structural flagellar proteins. A. Fluorescence images of wild-type, Δ*fimV*, Δ*flhF* and Δ*fleN* cells expressing FliF-GFP (left), FimV-GFP (center) or FliC^{S267C} (right). FM^{TM} 4-64 was used as membrane stain (red). **B.** Frequency of wild-type, Δ*fimV*, Δ*flhF* and Δ*fleN* cells bearing bipolar, unipolar or no polar FliF-GFP foci (left), FliM-GFP foci (center) or FliC^{S267C} filaments (right). **C.** Frequency of wild-type, Δ*fimV* and Δ*fleN* cells bearing ectopic FliF-GFP foci (left), FliM-GFP foci (center) or FliC^{S267C} filaments (right). Columns and error bars represent average and standard deviation of at least three separate replicates (n=500 cells). Stars denote *p*-values of the two-tailed Student's T test not assuming equal variance (*=$p<0.05$; **= $p<0.01$; ***= $p<0.001$; ****= $p<0.0001$).

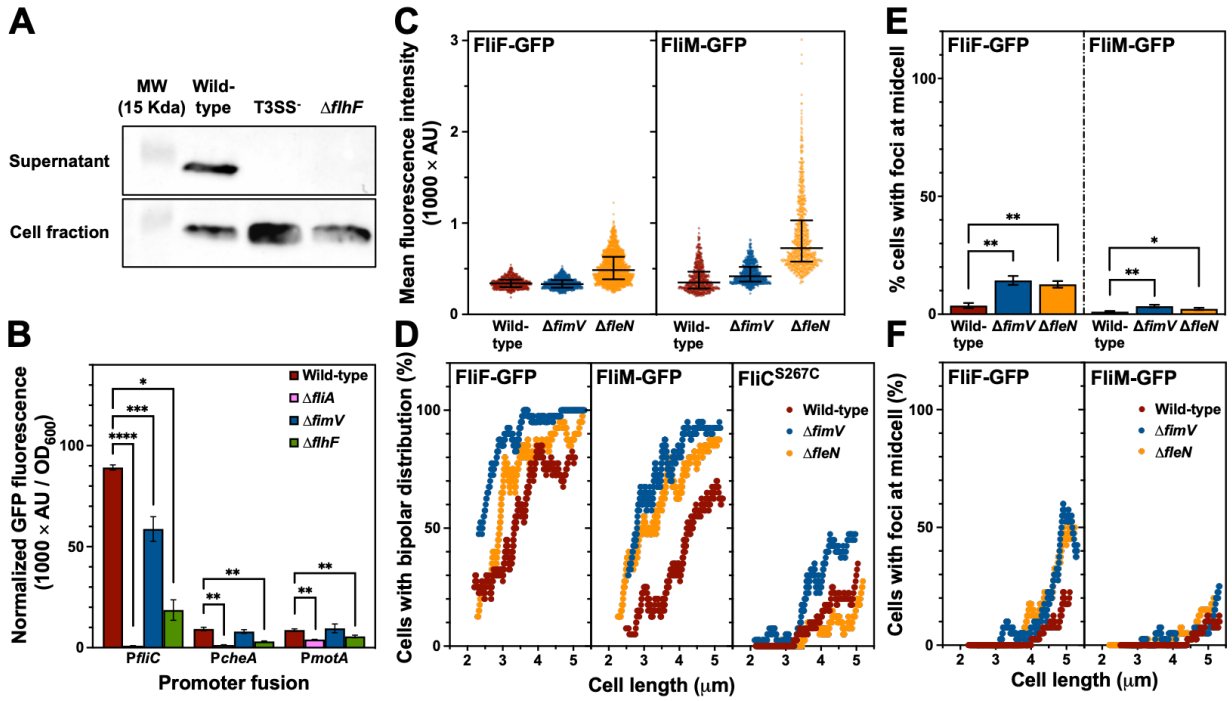

Figure 6. Analysis of the assembly of structural flagellar proteins. A. Western blot of FLAG-tagged FlgM in the supernatants (top) and cell fractions (bottom) of the wild-type, fT3SS$^-$ and Δ*flhF* strains. MW: molecular weight marker (15 kDa band shown). **B.** Normalized fluorescence from exponential cultures of wild-type, Δ*fliA*, Δ*fimV* and Δ*flhF* strains bearing transcriptional P*fliC-gfp*, P*cheA-gfp* or P*motA-gfp* fusions. Columns and error bars represent average and standard deviation of at least three separate replicates. Stars denote *p*-values of the two-tailed Student's T test not assuming equal variance (*=p<0.05; **= p<0.01; ***= p<0.001; ****= p<0.0001). **C**. Mean fluorescence intensity of polar FliF-GFP (left) or FliM-GFP (right) foci in wild-type, Δ*fimV* or Δ*fleN* cells bearing P*fliE-fliF-gfp* or P*fliL-fliM-gfp*. **D and F.** Frequency of wild-type, Δ*fimV* and Δ*fleN* cells displaying (**D**) bipolar FliF-GFP foci (left) FliM foci (center) or FliC filaments (right); or (**F**) midcell FliF-GFP (left) FliM (right) foci *vs*. cell length. Foci were scored from a set of 500 length-sorted cells of each strain in consecutive 40-cell windows and the frequency was plotted against the average length of each 40-cell set.**E.** Frequency of midcell FlIF-GFP (left) or FliM-GFP (right) foci in wild-type, Δ*fimV* and Δ*fleN* cells. Columns and error bars represent average and standard deviation of at least three separate replicates (n=500 cells). Stars denote *p*-values of the two-tailed Student's T test not assuming equal variance (*=p<0.05; **= p<0.01; ***= p<0.001; ****= p<0.0001).

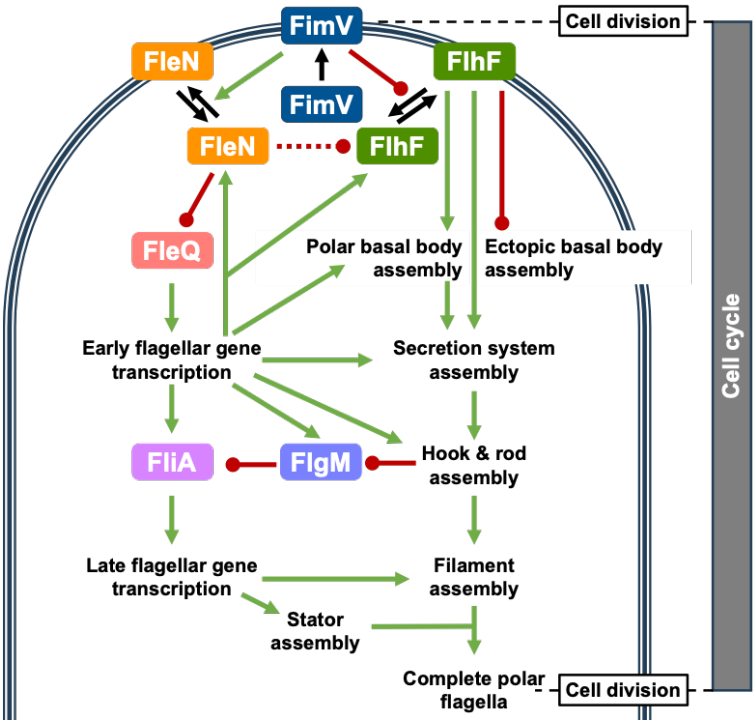

Figure 7. Circuit depicting the regulatory interactions between flagellar assembly regulators and structural components. A cell pole is represented and the vertical axis represents the timespan of a cell cycle. Regulatory proteins are shown as colored boxes. Transitions between free and cell pole-bound proteins are denoted by black arrows. Green arrows represent positive effects and red blocked lines represent negative effects. An uncharacterized negative interaction between FleN and FlhF is denoted by a dashed red blocked line.